Experimental Determination of Solubilities of Brucite [$Mg(OH)_2$(cr)] in Na_2SO_4 Solutions with Borate to High Ionic Strengths: Interactions of $MgB(OH)_4^+$ with Na_2SO_4

Yongliang Xiong [1*], Leslie Kirkes [1], Terry Westfall [1]

[1] Sandia National Laboratories (SNL), Carlsbad Programs Group, 4100 National Parks Highway, Carlsbad, NM 88220, USA

***Corresponding author email**: yxiong@sandia.gov

Abstract

In this work, a solubility study on brucite [$Mg(OH)_2$(cr)] in Na_2SO_4 solutions ranging from 0.01 to 1.8 mol•kg^{-1}, with 0.001 mol•kg^{-1} borate, has been conducted at 22.5°C. Based on the solubility data, the Pitzer interaction parameters for $MgB(OH)_4^+$—SO_4^{2-} and $MgB(OH)_4^+$—Na^+ along with the formation constant for $MgSO_4$(aq) are evaluated using the Pitzer model. The formation constant ($\log_{10} \beta_1^0 = 2.38 \pm 0.08$) for $MgSO_4$(aq) at 25°C and infinite dilution obtained in this study is in excellent agreement with the literature values.

The experimental data on the solubility of gypsum ($CaSO_4$•$2H_2O$), at 25°C, in aqueous solutions of $MgSO_4$ with ionic strengths up to ~11 mol•kg^{-1} were analyzed using models with and without considering the $MgSO_4$(aq) species. The model incorporating $MgSO_4$(aq) fits better to the experimental data than the model without $MgSO_4$(aq), especially in the ionic strength range beyond ~4 mol•kg^{-1}, demonstrating the need for incorporation of $MgSO_4$(aq) into the model to improve the accuracy.

INTRODUCTION

An accurate knowledge of solubilities of brucite ($Mg(OH)_2$) in sulfate solutions is important to numerous fields. In the field of nuclear waste management, brucite has become important to waste isolation projects owing to its use as engineered barriers for nuclear waste repositories. Crystalline MgO, which hydrates rapidly to brucite [1], is the only engineered barrier certified by the US Environmental Protection Agency (EPA) for the Waste Isolation Pilot Plant (WIPP) located near Carlsbad, New Mexico, USA (e.g., [1-2]). The WIPP is in a bedded salt formation. An $Mg(OH)_2$-based engineered barrier is also proposed for the German Asse salt mine repository [3]. Sulfate is a major species in some natural brines associated with salt formations. For instance, the sulfate concentrations in the two WIPP brines important to the performance assessment (PA), i.e., Generic Weep Brine (GWB) and U.S. Energy Research and Development Administration Well 6 (ERDA-6) are 0.203 $mol \bullet kg^{-1}$ and 0.187 $mol \bullet kg^{-1}$, respectively [1]. The sulfate concentrations in the Q-brine at the Asse are 0.2 $mol \bullet kg^{-1}$ [4]. In addition, the borate concentrations in the WIPP brines GWB and ERDA-6, are 0.178 $mol \bullet kg^{-1}$ (or 0.0445 $mol \bullet kg^{-1}$ if it is expressed as $B_4O_7^{2-}$) and 0.0704 $mol \bullet kg^{-1}$ (or 0.0176 $mol \bullet kg^{-1}$ if it is expressed as $B_4O_7^{2-}$), respectively. Therefore, accurate knowledge about the solubility of brucite in sulfate solutions is important to the performance of the engineered barrier. Finally, in the low level and intermediate level radioactive sulfate liquid waste (LLW and ILW) in Spain, the associated solutions are very rich in SO_4^{2-}, up to 2.2 $mol \bullet kg^{-1}$ [5]. Cements are proposed to be the waste form for such

46 LLW and ILW [5]. When portlandite [$Ca(OH)_2$(cr)], the major component of cements with
47 MgO being a minor constituent, is transformed into gypsum ($CaSO_4 \cdot 2H_2O$) in such
48 sulfate-rich environments, the solubility of gypsum in sulfate solutions in the presence of
49 Mg(II) will be important to the performance of cement waste form.

50 In the field of construction industry, Portland cement pastes are subject to $MgSO_4$
51 solutions attack (e.g., [6-8]). When such an attack occurs, brucite forms on the surface
52 almost immediately after cements are in contact with the solution [8]. As the molar volume
53 of $Mg(OH)_2$ is higher than that of portlandite [$Ca(OH)_2$] [9], the amounts of brucite formed
54 have direct impact on the deterioration of cements.

55 In the field of metallurgy and corrosion science, magnesium-based alloys are
56 widely used in various industries. In addition, magnesium is also used as magnesium-rich
57 primers to protect aluminum-based alloys (e.g., [10]). When magnesium-based alloys such
58 as AZ91D and AZ30, and magnesium-rich primers are corroded in sulfate solutions, brucite
59 forms (e.g., [11-15]). Therefore, accurate knowledge of brucite solubility in sulfate
60 solutions will provide a better understanding of corrosion behavior of magnesium-based
61 alloys and magnesium-rich primers, and hence enable researchers to predict the performance
62 of these alloys and primers when they are subject to corrosion in sulfate solutions.

63 As accurate knowledge of brucite solubility in sulfate-bearing solutions will impact
64 a wide range of fields, we investigate solubilities of brucite in Na_2SO_4 solutions in the

65 presence of borate, with a wide range of ionic strengths up to 5.4 mol•kg^{-1} in this work. We
66 performed long-term solubility measurements in our work, approaching equilibrium from the
67 direction of undersaturation in Na_2SO_4 solutions at the following concentrations: 0.01, 0.1,
68 0.5, 1.0, 1.5 and 1.8 mol•kg^{-1}, with a borate concentration of 0.001 mol•kg^{-1}. The objective
69 of this work is to investigate the specific interactions of $MgB(OH)_4^+$ with a Na_2SO_4 medium
70 based on the solubility of brucite in Na_2SO_4 solutions in the presence of borate. In the
71 previous studies ([16], and references therein), the specific interactions of brucite with a NaCl
72 medium have been investigated. Based on the experimental data from the current work, we
73 develop a Pitzer model to describe solubilities of brucite in Na_2SO_4 solutions in the presence
74 of borate, to high ionic strengths.

75

76

77 **EXPERIMENTAL METHODOLOGY**

78

79 All materials (Na_2SO_4, $Mg(OH)_2$, and H_3BO_3) used in this study are reagent grade
80 from Fisher Scientific. The purity of Na_2SO_4 was 99.99%. The purity of $Mg(OH)_2$ and
81 $H3BO_3$ was 99.9%. Deionized (DI) water with 18.3 MΩ was produced by a *Barnstead*
82 *NANOpure Water System* from Thermo Scientific. Degassed DI water was used for
83 preparation of all starting solutions. The degassed DI water was obtained by bubbling high
84 purity argon gas (purity 99.996%) from AIR GAS, Inc., through DI water for at least one hour,

85 following a procedure similar to that described by Wood et al. [17]. Starting solutions were
86 prepared such that the equilibrium solubility was approached from under-saturation with
87 respect to brucite. The experimental duration for reaching equilibrium with brucite has been
88 established before in NaCl solutions from both under- and super-saturation [16].
89 Solubility experiments approaching equilibrium from the direction of undersaturation
90 were conducted at six concentrations of Na_2SO_4, i.e., 0.010, 0.10, 0.50, 1.0, 1.5, and 1.8
91 mol•kg^{-1} Na_2SO_4, with 0.001 mol•kg^{-1} H_3BO_3. At each concentration of Na_2SO_4,
92 experiments were set-up in duplicate.
93 All experiments were conducted at room temperature (22.5 ± 0.5 °C). For each of
94 the experiments undersaturated with respect to brucite, 5 grams of $Mg(OH)_2$(cr) were placed
95 into a 150-mL polyethylene bottles containing 100-ml of a supporting solution (a Na_2SO_4
96 solution with 0.001 mol•kg^{-1} H_3BO_3).
97 The pH readings were measured with an Orion-Ross combination pH glass electrode,
98 coupled with an Orion Research EA 940 pH meter. Before each measurement, the pH meter
99 was calibrated with three pH buffers (pH 4, pH 7, and pH 10). In solutions with an ionic
100 strength higher than 0.10 mol•kg^{-1}, negative logarithms of hydrogen-ion concentrations on
101 molar scale (pcH) were determined from pH readings by using correction factors for Na_2SO_4
102 solutions determined before [18], which were re-analyzed [19]. Based on the equation in
103 Xiong et al. [20], pcHs are converted to negative logarithms of hydrogen-ion concentrations

104 on the molal scale (pH_m).

105 As described above, therefore, the pH scale adopted by this work was a concentration
106 scale in this work. The concentrations of hydrogen-ion were determined based on the
107 correction factors for converting pH readings to pcH, and then pH_m,

108 Solution samples were periodically withdrawn from experimental runs. Before
109 solution samples were taken, pH readings of experimental runs were measured. The sample
110 size was usually 3 mL. After a solution sample was withdrawn from an experiment and
111 filtered with a 0.2 μm syringe filter, the filtered solution was then weighed, acidified with
112 0.5 mL of concentrated TraceMetal® grade HNO_3 from Fisher Scientific, and finally diluted
113 to a volume of 10 mL with DI water. If subsequent dilutions were needed, aliquots were
114 taken from the first dilution samples for the second dilution, and aliquots of the second
115 dilution were then taken for further dilution.

116 The chemical analyses of solutions were performed with a Perkin Elmer dual-view
117 inductively coupled plasma-atomic emission spectrometer (ICP-AES)
118 (Perkin Elmer DV 3300). Calibration blanks and standards were precisely matched with
119 experimental matrices. The linear correlation coefficients of calibration curves in all
120 measurements were better than 0.9995. The analytical precision for ICP-AES was better
121 than 1.00% in terms of the relative standard deviation (RSD) based on replicate analyses.

122 Solid phase identification was performed by using a Bruker AXS, Inc., D8 Advance

X-ray diffractometer (XRD) with a Sol-X detector. XRD patterns were collected using CuKα radiation at a scanning rate of 1.33°/min for a 2θ range of 10–90°. There was no phase change as indicated by Figure 1A and 1B. The presence of thernardite [Na_2SO_4(cr)] in the XRD patterns for the experimental runs in 0.5, 1.0, 1.5 and 1.8 mol•kg^{-1} Na_2SO_4 (Figures 1A and 1B) was due to the fact that thernardite crystallized from the residual Na_2SO_4 solutions when the samples were dried for XRD analyses.

EXPERIMENTAL RESULTS

In all of the experiments, the solubility-controlling phase is brucite (Figures 1A and 1B). The experimental results including molalities of magnesium and pH_m for the solubility of brucite in aqueous solutions of sodium sulfate containing 0.001 mol•kg^{-1} H_3BO_3, are tabulated in Table 1. The durations of the experiments were up to 383 days. The experimental time was long enough to ensure the attainment of equilibrium. In Xiong [16], it has been demonstrated from both undersaturation and supersaturation experiments in NaCl and $MgCl_2$ solutions that the duration of experimental time for attainment of equilibrium was ~83 days (i.e., ~2000 hours).

In Figure 2 are shown the equilibrium total magnesium molalities [i.e., ΣMg(II)] (in a logarithmic scale) as a function of experimental time. Figure 2 shows the attainment of equilibrium, which is illustrated by the constant molalities of magnesium as a function of

142 experimental time, especially for the experiments at lower ionic strengths (i.e., 0.01 and 0.1
143 mol•kg^{-1} Na_2SO_4). However, there are some scatters in magnesium molality for the
144 experiments at higher ionic strengths (e.g., 1.5, 1.8 mol•kg^{-1} Na_2SO_4) owing to slight
145 variations in pH_m (Figure 3).

146 In Figure 3, pH_m as a function of experimental time is displayed. Figure 3 shows
147 that the pH_m generally varies from ~10.1 to ~10.3, which is within the usually combined
148 uncertainties from the procedure and the instrument. Of note, the procedural uncertainty in
149 measuring pH above pH 10 is ~0.15 [21]. The pH_m almost remains constant in the
150 experiments in lower ionic strength solutions (i.e., 0.01 and 0.1 mol•kg^{-1} Na_2SO_4) (Figure 3).
151 There are relatively higher variations in pH_m in the experiments in higher ionic strength
152 solutions (e.g., 1.8 mol•kg^{-1} Na_2SO_4), contributing to the scatters in molality of magnesium
153 for the respective experiments, as solubilities of brucite is pH_m-dependent, as suggested by
154 the following reaction,

155

156 $$Mg(OH)_2(cr) + 2H^+ \rightleftharpoons Mg^{2+} + 2H_2O(l) \quad (1)$$

157

158 In Reaction (1), the equilibrium quotient can be written as

159

160 $$Q = \frac{m_{\Sigma Mg(II)}}{(m_{H^+})^2} \quad (2)$$

161

162 Reaction (1) suggests that when m_{H^+} changes, magnesium concentrations will

163 correspondingly change.

164 In Figure 4, $\log \frac{m_{\Sigma Mg(II)}}{(m_{H^+})^2}$ is plotted versus experimental time. It can be seen that the

165 variations in $\log \frac{m_{\Sigma Mg(II)}}{(m_{H^+})^2}$ versus experimental time seem to be statistically indistinguishable,

166 which is consistent with what was observed in the literature. The experimental data for

167 short durations from McGee and Hostetler [22] in pure water at 25°C from the direction of

168 undersaturation are also plotted in Figure 4. The longest experimental run in their

169 experiments lasted for ~13 days (316 hours). In the enlarged insert for their data in Figure 4,

170 there are variations in $\log \frac{m_{\Sigma Mg(II)}}{(m_{H^+})^2}$ versus experimental time, but they are also statistically

171 indistinguishable. In Figure 4, the experimental data from [16] approaching equilibrium

172 from the direction of supersaturation started with a 0.1 mol•kg^{-1} $MgCl_2$ solution are also

173 plotted. The duration for that experimental run from [16], which lasted for up to 1,514 days,

174 was much longer than that in this work. After attainment of equilibrium at ~83 days for that

175 experimental run from supersaturation [16], Figure 4 shows that there are statistically

176 indistinguishable variations in in $\log \frac{m_{\Sigma Mg(II)}}{(m_{H^+})^2}$ versus experimental time, similar to those

177 present in this study.

178

THERMODYNAMIC MODELING

In this part, we present the thermodynamic model to describe the solubilities of brucite in Na_2SO_4 solutions in the presence of borate to high ionic strength. As the Pitzer activity coefficient model is valid to high ionic strengths, we adopt the Pitzer model as the framework.

In the modeling, the computer code, EQ3/6 Version 8.0a [23-24], is used as the modeling platform. The EQ3/6 Version 8.0a has been successfully utilized as the modeling platform in a number of previous studies at both ambient temperatures (e.g., [4, 25-27]) and at elevated temperatures up to 250^{o}C (e.g., [28-30]). The database containing all parameters necessary including thermodynamic properties for the modeling, is the Waste Isolation Pilot Plant (WIPP) thermodynamic database, data0.fm1 [31]. This database adopts the parameters for major ions from Harvie et al. [32].

In the model calculations, the experimental data were first employed to generate EQ3/6 Version 8.0a input files. Then, a script such as a Python script was generated to call the targeted parameters, and call EQ3/6. The minimization subroutine in the script automatically compares differences between experimental values and model-predicted values produced by a set of inputted parameters in each iteration. The iteration is complete when the difference is finally minimized.

197 In Figures 5 and 6, solubilities of brucite as a function of ionic strengths in Na_2SO_4
198 solutions as a function of pH_m predicted by using the key parameters of the model without
199 $MgSO_4(aq)$ listed in Table 2 are shown in comparison with the experimental data. These
200 parameters, mainly concerning the interactions with SO_4^{2-}, are from Harvie et al. [32].
201 Figures 5-6 illustrate that these parameters without $MgSO_4(aq)$ do not adequately describe the
202 experimental data.

203 As numerous studies suggest the existence of the complex, $MgSO_4(aq)$ (e.g., [33-36),
204 we explicitly introduce $MgSO_4(aq)$ into the model. The formation reaction for $MgSO_4(aq)$
205 can be expressed as,

206 $$Mg^{2+} + SO_4^{2-} \rightleftharpoons MgSO_4(aq) \qquad (3)$$

207 The formation constant ($\log_{10} \beta_1^0$) for Reaction 1 obtained by this study is 2.38 ± 0.08
208 (Table 3). Notice that the uncertainty also includes the minor corrections from 22.5°C to the
209 standard temperature of 25°C. In addition, the interaction parameters for
210 $MgB(OH)_4^+$—SO_4^{2-} and $MgB(OH)_4^+$—Na^+ are also evaluated (Table 3).

211 The formation constant for $MgSO_4(aq)$ obtained by this is in excellent agreement
212 with the values in literature (e.g., [41-43]). For instance, Nair and Nancollas [41] obtained a
213 value of 2.13 for $\log_{10} \beta_1^0$ based on conductivity measurement. Kester [42] calculated a
214 value of 2.32 for $\log_{10} \beta_1^0$ based on potentiometric measurements. Noticeably, Kratsis et al.
215 [43] determined the formation constant of $MgSO_4(aq)$ via a potentiometric study with a

magnesium ion-selective electrode. The supporting electrolyte for their work was CsCl with ionic strengths up to 6.0 mol•dm^{-3}. The $\log_{10}\beta_1^0$ obtained by Kratsis et al. [43] using the Debye-Hückel equation for extrapolation to infinite dilution was 2.38 ± 0.03.

The solubilities of brucite as a function of pH_m over a range of ionic strengths predicted by the model with $MgSO_4(aq)$ are compared with the experimental data in Figures 7 and 8 for a more detailed view. It is clear from Figures 7 and 8 that the model reproduces the experimental data with fair agreement, especially in high ionic strength range.

In the presence of Mg(II)-bearing solutions, the formation of $MgSO_4(aq)$ can influence solubilities of gypsum ($CaSO_4•2H_2O$), as total sulfate concentrations are expected to increase when gypsum is dissolved in a Mg-containing medium,

$$CaSO_4•2H_2O(cr) \rightleftharpoons Ca^{2+} + SO_4^{2-} + 2H_2O(l) \quad (4)$$

Based on solubility data of gypsum in mixtures of NaCl and $MgCl_2$, dominated by NaCl with $MgCl_2$ to 0.325 mol•kg^{-1} and with total ionic strengths up to 5.83 mol•kg^{-1} from Ostruff and Melter [40], the interaction between $MgSO_4(aq)$ and Cl^- is evaluated (Table 3). In the work of Ostruff and Melter [40], they measured gypsum solubilities in mixtures of NaCl and $MgCl_2$ at 28°C. The molality of NaCl ranges from 0.0501 mol•kg^{-1} to 5.50 mol•kg^{-1}. The molality of $MgCl_2$ ranges from 0.0100 mol•kg^{-1} to 0.325 mol•kg^{-1}. In this work, the interaction between $MgSO_4(aq)$ and Cl^- is modeled based on their experimental data at 28°C, and other parameters including the solubility constant of gypsum are from the data0.fm1 [31].

In Figure 9, solubilities of gypsum predicted by using the model developed in this study are compared with the experimental data in mixtures of NaCl and $MgCl_2$. Figure 9 shows that the predicted values are in good agreement with the experimental values.

As a validation test, the model predicted solubilities of gypsum in $MgSO_4$ solutions with a wide range of ionic strengths at 25°C are compared with model-independent experimental solubilities in the same medium at the same temperature (Figure 10). The model-independent experimental data include Dietriech [44], Harkins and Paine [45], Kolosov [46], Wollmann and Voigt [47], Tanji [48], and Friedel [49]. In the model predicted values, they include those predicted by the model without $MgSO_4$(aq), and those with $MgSO_4$(aq). It is clear from Figure 10 that these two models have similar accuracy up to an ionic strength of ~4 mol•kg^{-1}. However, above an ionic strength of 4 mol•kg^{-1}, the model with $MgSO_4$(aq) is in better agreement with model-independent experimental data than the model without $MgSO_4$(aq) (Figure 10), independently demonstrating that the incorporation of $MgSO_4$(aq) improves the accuracy of the model.

CONCLUSIONS

In this study, we conducted long-term solubility measurements on brucite at 22.5°C in Na_2SO_4 solutions from 0.01 mol•kg^{-1} to 1.8 mol•kg^{-1} with 0.001 mol•kg^{-1} H_3BO_3. Based on experimental data, we evaluated a set of Pitzer parameters along with the stability constant of $MgSO_4$(aq) ($\log_{10} \beta_1^0$) as 2.38 ± 0.08, which is in excellent agreement with the literature values. The model developed in this study can describe not only brucite solubilities in sulfate-bearing solutions, but also gypsum solubilities in mixtures of NaCl and $MgCl_2$ to I_m ~6 mol•kg^{-1}, dominated by NaCl with $MgCl_2$ up to ~0.4 mol•kg^{-1}, and in $MgSO_4$ solutions up to I_m ~13 mol•kg^{-1}.

ACNOWLEDGEMENTS

Sandia National Laboratories is a multi-mission laboratory managed and operated by Sandia Corporation, a wholly owned subsidiary of Lockheed Martin Corporation, for the U.S. Department of Energy's National Nuclear Security Administration under contract DE-AC04-94AL85000. This research is funded by the WIPP programs administered by the Office of Environmental Management (EM) of the U.S. Department of Energy. RAA578404. Jandi Knox, Cassie Marrs, and Heather Burton are thanked for their contributions. The laboratory assistance from Lindsay Day, Diana Goulding, Brittany Hoard, Chase Kicker, Danelle Morrill, Cassandra Marrs, Rachael Roselle, Mathew Stroble,

William Sullvan, Kira Vincent, and Yoni Xiong is gratefully acknowledged. The authors are grateful to the three journal reviewers for their insightful and thorough reviews, which have improved the presentation of the article, and to Dr. Magdalena Bendová, the journal editor, for her time and editorial efforts. The authors wish to thank Dr. Earle Waghorne, Editor-in-Chief, for his invitation to the first and senior author to contribute to the special issue of ISSP-17.

REFERENCES

1. Xiong, Y.-L., Lord, A.C.: Experimental investigations of the reaction path in the MgO–CO_2–H_2O system in solutions with various ionic strengths, and their applications to nuclear waste isolation. Applied Geochemistry **23**, 1634–1659 (2008)
2. Krumhansl, J.L., Panenguth, H.W., Zhang, P.-C., Kelly, J.W., Anderson, H.L., and Hardesty, J.O.: Behavior of MgO as a CO_2 scavenger at the Waste Isolation Pilot Plant (WIPP), Carlsbad, New Mexico. Material Research Society Symposium Proceedings 608, 155–160 (2000)
3. Schüssler, W., Metz, V., Kienzler, B., Vejmelka, P.: Geochemically based source term assessment for the Asse salt mine: comparison of modeling and experimental results (Abstract). Programs and Abstracts of Materials Research Society Annual Meeting at Boston, MA, p.713 (2002)
4. Schuessler, W., Kienzler, B., Wilhelm, S., Neck, V. and Kim, J.I.: Modeling of near field actinide concentrations in radioactive waste repositories in salt formations: Effect of buffer materials. Mat. Res. Soc. Symp. Proc. Vol. 663, p. 791 (2000)
5. Guerrero, A., Goni, S., Hernandez, M.-S.: Thermodynamic solubility constant of $Ca(OH)_2$ in simulated radioactive sulfate liquid waste. Journal of American Ceramics Society **83**, 882 (2000)
6. Moukwa, M.: Characteristics of the attack of cement paste by $MgSO_4$ and $MgCl_2$ from the pore structure measurements. Cement and Concrete Research **20,** 148–158 (1990)
7. Gollop, R.S. and Taylor, H.F.W.: Microstructural and microanalytical studies of sulfate attack. IV. Reactions of a slag cement paste with sodium and magnesium sulfate solutions. Cement and Concrete Research **26**, 1013–1028 (1996)
8. Santhanam, M., Cohen, M.D. and Olek, J.: Mechanism of sulfate attack: A fresh look Part 1: Summary of experimental results. Cement and concrete research **32**, 915–921 (2001)
9. Tumidajski, P.J., and Chan, G.W.: Durability of high performance concrete in magnesium brine. Cement and concrete research **26**, 557–565 (1996)
10. Battocchi, D., Simoes, A.M., Tallman, D.E. and Bierwagen, G.P.: Comparison of testing solutions on the protection of Al-alloys using a Mg-rich primer. Corrosion Science **48**, 2226–2240 (2006)
11. Yang, L.J., Wei, Y.H., Hou, L.F. and Zhang, D.: Corrosion behaviour of die-cast AZ91D magnesium alloy in aqueous sulphate solutions. Corrosion Science **52**, 345–351 (2010)
12. Tian, Y., Yang, L.J., Li, Y.F., Wei, Y.H., Hou, L.F., Li, Y.G. and Murakami, R.I.: Corrosion behaviour of die-cast AZ91D magnesium alloys in sodium sulphate solutions with different pH values. Transactions of Nonferrous Metals Society of China **21**,

912–920 (2011)
13. King, A.D., Kannan, B. and Scully, J.R.: Environmental Degradation of a Mg-Rich Primer in Selected Field and Laboratory Environments: Part 1-Without a Topcoat. Corrosion **70**, 512–535 (2014)
14. Zeng, R.C., Hu, Y., Guan, S.K., Cui, H.Z. and Han, E.H.: Corrosion of magnesium alloy AZ31: The influence of bicarbonate, sulphate, hydrogen phosphate and dihydrogen phosphate ions in saline solution. Corrosion Science **86**, 171–182 (2014)
15. Lin, J., Battocchi, D. and Bierwagen, G.: Degradation of magnesium rich primers over AA2024-T3 during constant immersion in different solutions. Corrosion **73**, 408–416 (2017)
16. Xiong, Y.-L.: Thermodynamic properties of brucite determined by solubility studies and their significance to nuclear waste isolation. Aquatic Geochemistry **14**, 223–238 (2008)
17. Wood, S.A., Palmer, D.A., Wesolowski, D.J., and Bénézeth, P.: In Hellmann, R. and Wood, S.A., ed., Special Publication 7, The Geochemical Society, pp. 229–256 (2002)
18. Rai, D., Felmy, A.R., Juracich, S.I., Rao, F.F.: Estimating the Hydrogen Ion Concentration in Concentrated NaCl and Na_2SO_4 Electrolytes. SAND94-1949. Albuquerque, NM: Sandia National Laboratories (1995)
19. Roselle, G.: Determination of pC_{H+} Correction Factors in Brines. Work Carried Out under the Analysis Plan for Determination of pC_{H+} Correction Factors in Brines, AP157, Rev 0. Sandia National Laboratories, Carlsbad, NM (2011)
20. Xiong, Y.-L., Deng, H.-R., Nemer, M., and Johnsen, S.: Experimental determination of the solubility constant for magnesium chloride hydroxide hydrate ($Mg_3Cl(OH)_5{\cdot}4H_2O$), phase 5) at room temperature, and its importance to nuclear waste isolation in geological repositories in salt formations. Geochimica et Cosmochimica Acta **74**, 4605–46011 (2010)
21. Leito, I., Strauss, L., Koort, E. and Pihl, V.: Estimation of uncertainty in routine pH measurement. Accreditation and Quality Assurance: Journal for Quality, Comparability and Reliability in Chemical Measurement **7**, 242–249 (2002)
22. McGee, K.A. and Hostetler, P.B.: Activity-product constants of brucite from 10 to 90ºC. Journal of Research of US Geological Survey **5**, 227–233 (1977)
23. Wolery, T.J., Xiong, Y.-L., and Long, J.: Verification and Validation Plan/Validation Document for EQ3/6 Version 8.0a for Actinide Chemistry, Document Version 8.10. Carlsbad, NM: Sandia National laboratories. ERMS 550239 (2010)
24. Xiong, Y.-L.: WIPP Verification and Validation Plan/Validation Document for EQ3/6 Version 8.0a for Actinide Chemistry, Revision 1, Document Version 8.20. Supersedes ERMS 550239. Carlsbad, NM. Sandia National Laboratories. ERMS 555358 (2011)

25. Xiong, Y.-L., Kirkes, L., and Westfall, T.: Experimental Determination of Solubilities of Sodium Tetraborate (Borax) in NaCl Solutions, and A Thermodynamic Model for the Na–$B(OH)_3$–Cl–SO_4 System to High Ionic Strengths at 25 °C. American Mineralogist **98**, 2030–2036 (2013).
26. Xiong, Y.-L., Kirkes, L., Westfall, T., Roselle, R.: Experimental determination of solubilities of lead oxalate (PbC_2O_4(cr)) in a NaCl medium to high ionic strengths, and the importance of lead oxalate in low temperature environments. Chemical Geology **342**, 128–137 (2013)
27. Xiong, Y.-L.: Experimental determination of lead carbonate solubility at high ionic strengths: a Pitzer model description. Monatshefte für Chemie-Chemical Monthly **146**, 1433–1443 (2015)
28. Xiong, Y.-L.: An Aqueous Thermodynamic Model for Solubility of Potassium Ferrate in Alkaline Solutions to High Ionic Strengths at 283.15 K to 333.15 K. Journal of Solution Chemistry **42**, 1393–1403 (2013)
29. Xiong, Y.-L.: A Thermodynamic Model for Silica and Aluminum in Alkaline Solutions with High Ionic Strength at Elevated Temperatures up to 100 °C : Applications to Zeolites. American Mineralogist **98**, 141–153 (2013).
30. Xiong, Y.-L.: A Pitzer model for the Na-$Al(OH)_4$-Cl-OH system and solubility of boehmite (AlOOH) to high ionic strength and to 250°C. Chemical Geology **373**, 37–49 (2014)
31. Xiong, Y.-L.: Release of EQ3/6 Database DATA0.FM1. Carlsbad, NM: Sandia National Laboratories. ERMS 555152 (2011)
32. Harvie, C.E., Moller, N., Weare, J.H.: The prediction of mineral solubilities in natural waters: The Na-K-Mg-Ca-H-Cl-SO_4-OH-HCO_3-CO_3-CO_2-H_2O system to high ionic strengths at 25°C. Geochimica et Cosmochimica Acta **48**, 723–751 (1984)
33. Daly, F.P., Brown, C.W. and Kester, D.R.: Sodium and magnesium sulfate ion pairing: Evidence from Raman spectroscopy. The Journal of physical chemistry ***76***, 3664–3668 (1972)
34. Katayama, S.: Conductometric determination of ion-association constants for magnesium and nickel sulfates in aqueous solutions at various temperatures between 0°C and 45°C. Bulletin of the Chemical Society of Japan **46,** 106–109 (1973)
35. Elgquist, B. and Wedborg, M.: Stability of ion pairs from gypsum solubility degree of ion pair formation between the major constituents of seawater. Marine Chemistry **3**, 215–225 (1975)
36. Rudolph, W.W., Irmer, G. and Hefter, G.: Raman spectroscopic investigation of speciation in $MgSO_4$(aq). Physical Chemistry Chemical Physics **5**, 5253–5261(2003)
37. Domski, P.S.: Memo AP-173, EQ3/6 Database Update: DATA0.FM2. Carlsbad, NM: Sandia National Laboratories. ERMS 564914 (2015)

38. Xiong, Y.-L., and Domski, P.S.: Updating the WIPP Thermodynamic Database, Revision 1, Supersedes ERMS 565730. Carlsbad, NM: Sandia National Laboratories. ERMS 566047 (2016)
39. Choppin G. R., Bond A. H., Borkowski M., Bronikowski M. G., Chen J.-F., Lis S., Mizera J. Pokrovsky O. S., Wall N. A., Xia Y.-X. and Moore, R. C.: Waste Isolation Pilot Plant Actinide Source Term Test Program: Solubility Studies and Development of Modeling Parameters. Sandia National Laboratories Report. SAND99-0943 (2001)
40. Ostroff, A. G. and Metler, A. V., Solubility of calcium sulfate dihydrate in the system NaCl-$MgCl_2$-H_2O from 28^0 to 70^0C. Journal of Chemical And Engineering Data **11**, 346–350 (1966)
41. Nair, V.S.K. and Nancollas, G.H.: Thermodynamics of ion association. Part IV. Magnesium and zinc sulphates. Journal of the Chemical Society (Resumed), 3706–3710 (1958)
42. Kester, D. R.: Ph.D. Thesis, Oregon State University, Corvallis (1969).
43. Kratsis, S., Hefter, G., May, P.: Potentiometric study of the sssociation of magnesium and sulfate ions at 25ºC in high ionic strength media. Journal of Solution Chemistry **30**, 19–29 (2001)
44. Dietriech, H.G.: Kaminer Handbuch der Balneologie, Vol. 1, p. 205 (1916)
45. Harkins, W. D.; Paine, H. M.: Intermediate and complex ions. V. The solubility product and activity of the ions in bi-bivalent salts. Journal of American Chemical Society **41**, 1155–1168 (1919)
46. Kolosov, A. S.: Isotherms of the system $MgSO_4$-$CaSO_4$-H_2O at 25°C. Trudy Khim.-Met. Inst., Akad. Nauk S.S.S.R., Zapadno-Sibir. Filial **35**, 29–38 (1958).
47. Wollmann, G. and Voigt, W.: Solubility of gypsum in MSO_4 solutions (M= Mg, Mn, Co, Ni, Cu, Zn) at 298.15 K and 313.15 K. Journal of Chemical & Engineering Data **53**, 1375–1380 (2008).
48. Tanji, K.K.: Solubility of gypsum in aqueous electrolytes as affected by ion association and ionic strengths up to 0.15 M and at 25 deg. Environmental Science & Technology **3**, 656–661 (1969)
49. Friedel, B.: Gypsum solubilities in aqueous systems containing NaCl, $MgCl_2$, Na_2SO_4, and $MgSO_4$. Zeitschrift Fur Pflanzenernahrung Und Bodenkunde **141**, 337–346 (1978)

Table1. Experimental results concerning solubility of brucite ($Mg(OH)_2$(cr)), as total magnesium molality, in Na_2SO_4 solutions with 0.001 mol•kg^{-1} H_3BO_3, at 22.5 ± 0.5 °C.

Experimental Number	Supporting Medium, $m_{Na_2SO_4}$/ mol•kg^{-1}	Experiment time, days	pH_m*	Solubility of brucite, $m_{Mg,total}$/mol•kg^{-1},
$MgB(OH)_4$-0.01SO_4-1	0.010	233	10.13	2.10E-03
$MgB(OH)_4$-0.01SO_4-2	0.010	233	10.14	2.11E-03
$MgB(OH)_4$-0.1SO_4-1	0.10	233	10.20	2.87E-03
$MgB(OH)_4$-0.1SO_4-2	0.10	233	10.23	2.80E-03
$MgB(OH)_4$-0.5SO_4-1	0.50	233	10.17	3.65E-03
$MgB(OH)_4$-0.5SO_4-2	0.50	233	10.15	3.60E-03
$MgB(OH)_4$-1.0SO_4-1	1.0	233	10.12	3.87E-03
$MgB(OH)_4$-1.0SO_4-2	1.0	233	10.12	3.88E-03
$MgB(OH)_4$-1.5SO_4-1	1.5	233	10.16	4.19E-03
$MgB(OH)_4$-1.5SO_4-2	1.5	233	10.16	2.80E-03
$MgB(OH)_4$-1.8SO_4-1	1.8	233	10.21	4.56E-03
$MgB(OH)_4$-1.8SO_4-2	1.8	233	10.21	4.67E-03
$MgB(OH)_4$-0.01SO_4-1	0.010	285	10.17	2.01E-03
$MgB(OH)_4$-0.01SO_4-2	0.010	285	10.18	2.01E-03
$MgB(OH)_4$-0.1SO_4-1	0.10	285	10.28	2.72E-03
$MgB(OH)_4$-0.1SO_4-2	0.10	285	10.29	2.72E-03
$MgB(OH)_4$-0.5SO_4-1	0.50	285	10.24	3.47E-03
$MgB(OH)_4$-0.5SO_4-2	0.50	285	10.25	3.43E-03
$MgB(OH)_4$-1.0SO_4-1	1.0	285	10.19	3.71E-03
$MgB(OH)_4$-1.0SO_4-2	1.0	285	10.20	3.68E-03
$MgB(OH)_4$-1.5SO_4-1	1.5	285	10.24	3.91E-03
$MgB(OH)_4$-1.5SO_4-2	1.5	285	10.24	3.87E-03
$MgB(OH)_4$-1.8SO_4-1	1.8	285	10.30	4.03E-03
$MgB(OH)_4$-1.8SO_4-2	1.8	285	10.31	4.22E-03
$MgB(OH)_4$-0.01SO_4-1	0.010	335	10.16	1.93E-03
$MgB(OH)_4$-0.01SO_4-2	0.010	335	10.18	1.95E-03
$MgB(OH)_4$-0.1SO_4-1	0.10	335	10.25	2.72E-03
$MgB(OH)_4$-0.1SO_4-2	0.10	335	10.25	2.72E-03

$MgB(OH)_4$-0.5SO_4-1	0.50	335	10.17	3.72E-03
$MgB(OH)_4$-0.5SO_4-2	0.50	335	10.17	3.68E-03
$MgB(OH)_4$-1.0SO_4-1	1.0	335	10.09	4.19E-03
$MgB(OH)_4$-1.0SO_4-2	1.0	335	10.07	4.13E-03
$MgB(OH)_4$-1.5SO_4-1	1.5	335	10.11	4.38E-03
$MgB(OH)_4$-1.5SO_4-2	1.5	335	10.08	4.39E-03
$MgB(OH)_4$-1.8SO_4-1	1.8	335	10.15	4.77E-03
$MgB(OH)_4$-1.8SO_4-2	1.8	335	10.16	4.98E-03
$MgB(OH)_4$-0.01SO_4-1	0.010	383	10.21	1.95E-03
$MgB(OH)_4$-0.01SO_4-2	0.010	383	10.22	1.99E-03
$MgB(OH)_4$-0.1SO_4-1	0.10	383	10.29	2.61E-03
$MgB(OH)_4$-0.1SO_4-2	0.10	383	10.27	2.53E-03
$MgB(OH)_4$-0.5SO_4-1	0.50	383	10.28	2.80E-03
$MgB(OH)_4$-0.5SO_4-2	0.50	383	10.22	2.86E-03
$MgB(OH)_4$-1.0SO_4-1	1.0	383	10.20	3.02E-03
$MgB(OH)_4$-1.0SO_4-2	1.0	383	10.21	2.99E-03
$MgB(OH)_4$-1.5SO_4-1	1.5	383	10.18	3.28E-03
$MgB(OH)_4$-1.5SO_4-2	1.5	383	10.17	3.10E-03
$MgB(OH)_4$-1.8SO_4-1	1.8	383	10.23	3.23E-03
MgB(OH)4-1.8SO4-2	1.8	383	10.23	3.45E-03

435 * Negative logarithms of hydrogen ion concentrations on a molal scale, $mol \bullet kg^{-1}$.

436

437 Table 2. Key parameters without $MgSO_4$(aq) describing solubility of brucite in Na_2SO_4
438 solutions with borate at 25°C*
439

Pitzer Binary Parameters				
Species, *i*	Species, *j*	$\beta^{(0)}$	$\beta^{(1)}/\beta^{(2)}$	C^{ϕ}
Mg^{2+}	SO_4^{2-}	0.221	3.343/-37.23	0.025
Na^{+}	SO_4^{2-}	0.01958	1.113	0.00497
Na^{+}	OH^{-}	0.0864	0.253	0.0044
Pitzer Mixing Parameters				
Species, *i*	Species, *j*	Species, *k*	θ_{ij}	Ψ_{ijk}
Mg^{2+}	Na^{+}	SO_4^{2-}	0.07	–0.015
Equilibrium constants at infinite dilution for dissolution reaction of brucite and dissociation reactions of $MgOH^{+}$ and $MgB(OH)_4^{+}$				
Reactions			$\log_{10} K^0$	
$Mg(OH)_2(cr) + 2H^{+} \rightleftarrows Mg^{2+} + 2H_2O(l)$			17.05 ± 0.20 [16]	
$MgOH^{+} + H^{+} \rightleftarrows Mg^{2+} + H_2O(l)$			11.8091	
$MgB(OH)_4^{+} \rightleftarrows Mg^{2+} + B(OH)_4^{-}$			–1.3993	

440 Unless otherwise noted, parameters are from the WIPP thermodynamic database, data0.fm1
441 [31]
442
443
444

Table 3. Key parameters with $MgSO_4$(aq) describing solubility of brucite in Na_2SO_4 solutions with borate at 25°C*

Pitzer Binary Parameters				
Species, *i*	Species, *j*	$\beta^{(0)}$	$\beta^{(1)}/\beta^{(2)}$	C^{ϕ}
Mg^{2+}	SO_4^{2-}	0.221	3.343/-37.23	0.025
Na^+	SO_4^{2-}	0.01958	1.113	0.00497
Na^+	OH^-	0.0864	0.253	0.0044
$MgB(OH)_4^+$	SO_4^{2-}	0.7806 (P.W.)	1.74** (P.W.)	0 (P.W.)
Pitzer Parameters for Neutral Species and Mixing				
Species, *i*	Species, *j*	Species, *k*	θ_{ij} or λ_{ij}	Ψ_{ijk}
$MgSO_4$(aq)	Cl^-		0.32 (P.W.)	
Mg^{2+}	Na^+	SO_4^{2-}	0.07	–0.015
Na^+	$MgB(OH)_4^+$		–0.2975 (P.W.)	
Equilibrium constants at infinite dilution for dissolution reaction of brucite and dissociation reactions of $MgOH^+$, $MgB(OH)_4^+$ and $MgSO_4$(aq)				
Reactions			$\log_{10} K^0$	
$Mg(OH)_2$(cr) + $2H^+ \rightleftarrows Mg^{2+} + 2H_2O$(l)			17.05 ± 0.20 [16]	
$MgOH^+ + H^+ \rightleftarrows Mg^{2+} + H_2O$(l)			11.8091	
$MgB(OH)_4^+ \rightleftarrows Mg^{2+} + B(OH)_4^-$			–1.3993	
$MgSO_4$(aq) $\rightleftarrows Mg^{2+} + SO_4^{2-}$			–2.38 ± 0.08 (P.W.)	

*Unless otherwise noted below, values without annotations are the default value from DATA0.FM1 [31], which is based on Harvie et al. [32] for major ions.

** This value was not evaluated. It was set to the average value for 1:2 and 2:1 interactions from Choppin et al. [39].

P.W.: Present Work.

454 Figure Captions
455
456 Figure 1. XRD patterns for the experiments conducted in this study after the experimental
457 runs. A. XRD patterns for all experiments with Replicate 1. B. XRD patterns for all
458 experiments with Replicate 2. The XRD standards for brucite [$Mg(OH)_2$(cr)] (in black) and
459 thernardite [Na_2SO_4(cr)] (in red) are from PDF-4+ 2016 (Software Version 4.16.04, Database
460 Version 4.1605) of the International Center for Diffraction Data (ICDD). Notice that the
461 peaks for thernardite appeared in the XRD patterns for the experimental runs in 0.5, 1.0, 1.5
462 and 1.8 mol•kg^{-1} Na_2SO_4, because thernardite crystallized from the residual Na_2SO_4 solutions
463 when the samples were dried.
464
465 Figure 2. A plot showing molalities of magnesium in equilibrium with brucite as a function
466 of experimental time
467
468 Figure 3. A plot showing pH_m/ mol•kg^{-1} in equilibrium with brucite as a function of
469 experimental time.
470
471 Figure 4. A plot showing $\log \frac{[m_{Mg(II)}]_{tot}}{(m_{H^+})^2}$ (i.e., $\log[m_{Mg(II)}]_{tot} + 2pH_m$) as a function of
472 experimental time. Of note, the experimental data from McGee and Hostetler [22] was
473 started with pure water at 25°C.
474
475 Figure 5. A plot showing molalities of magnesium in equilibrium with brucite as a function
476 of pH_m in Na_2SO_4 solutions ranging from 0.01 mol•kg^{-1} to 0.5 mol•kg^{-1}, in comparison with
477 the predicted values using the model without $MgSO_4$(aq).
478
479 Figure 6. A plot showing molalities of magnesium in equilibrium with brucite as a function
480 of pH_m in Na_2SO_4 solutions ranging from 1.0 mol•kg^{-1} to 1.8 mol•kg^{-1}, in comparison with
481 the predicted values using the model without $MgSO_4$(aq).
482
483 Figure 7. A plot showing molalities of magnesium in equilibrium with brucite as a function
484 of pH_m in Na_2SO_4 solutions ranging from 0.01 mol•kg^{-1} to 0.5 mol•kg^{-1}, in comparison with
485 the predicted values using the model with $MgSO_4$(aq). The predicted values were generated
486 using the database, DATA0.FM2 [37-38].
487
488 Figure 8. A plot showing molalities of magnesium in equilibrium with brucite as a function
489 of pH_m in Na_2SO_4 solutions ranging from 1.0 mol•kg^{-1} to 1.8 mol•kg^{-1}, in comparison with

the predicted values using the model with $MgSO_4$(aq). The predicted values were generated using the database, DATA0.FM2 [37-38].

Figure 9. A plot showing solubilities of gypsum as a function of ionic strength in the mixtures of NaCl and $MgCl_2$.

Figure 10. A plot showing solubilities of gypsum as a function of ionic strength in the $MgSO_4$ solutions. All of the experimental data are model-independent.

500

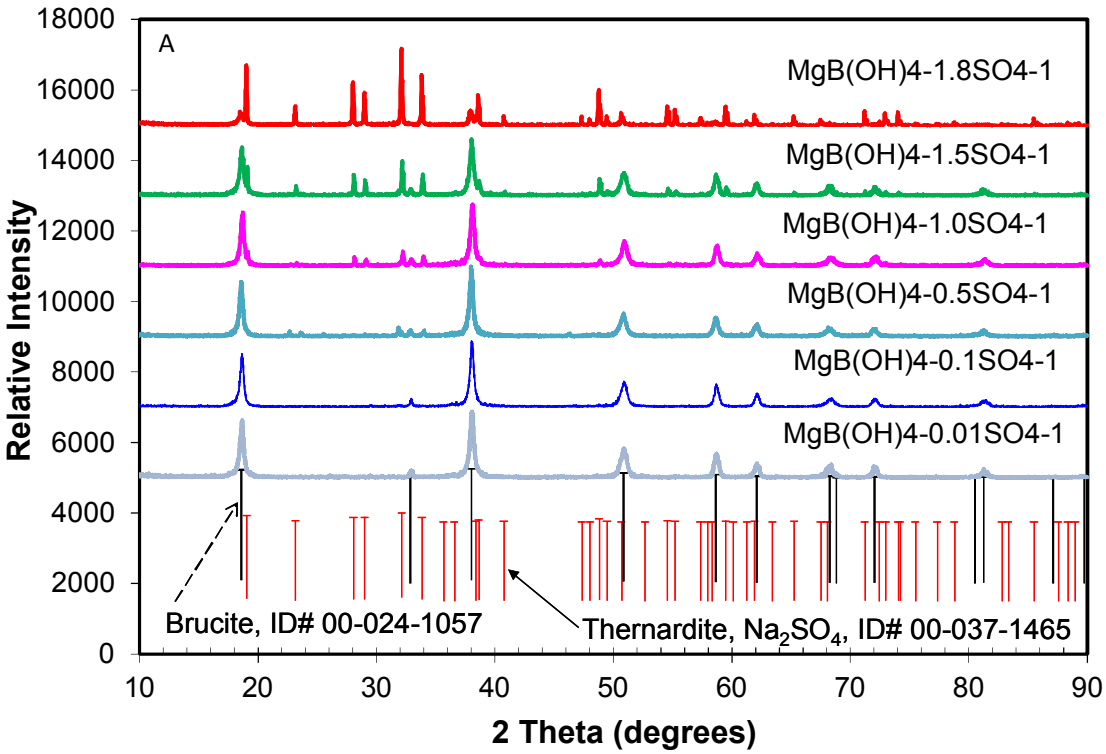

501

502 Figure 1 A

503

504

505

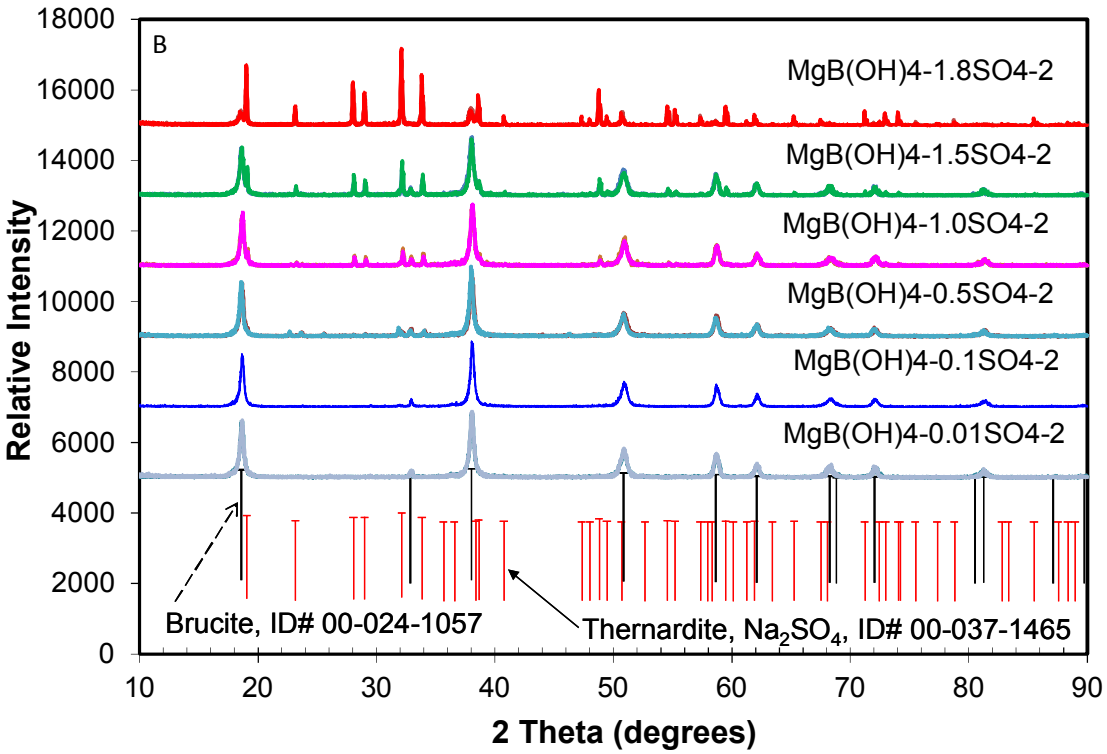

506

507

508 Figure 1B

509

510

511

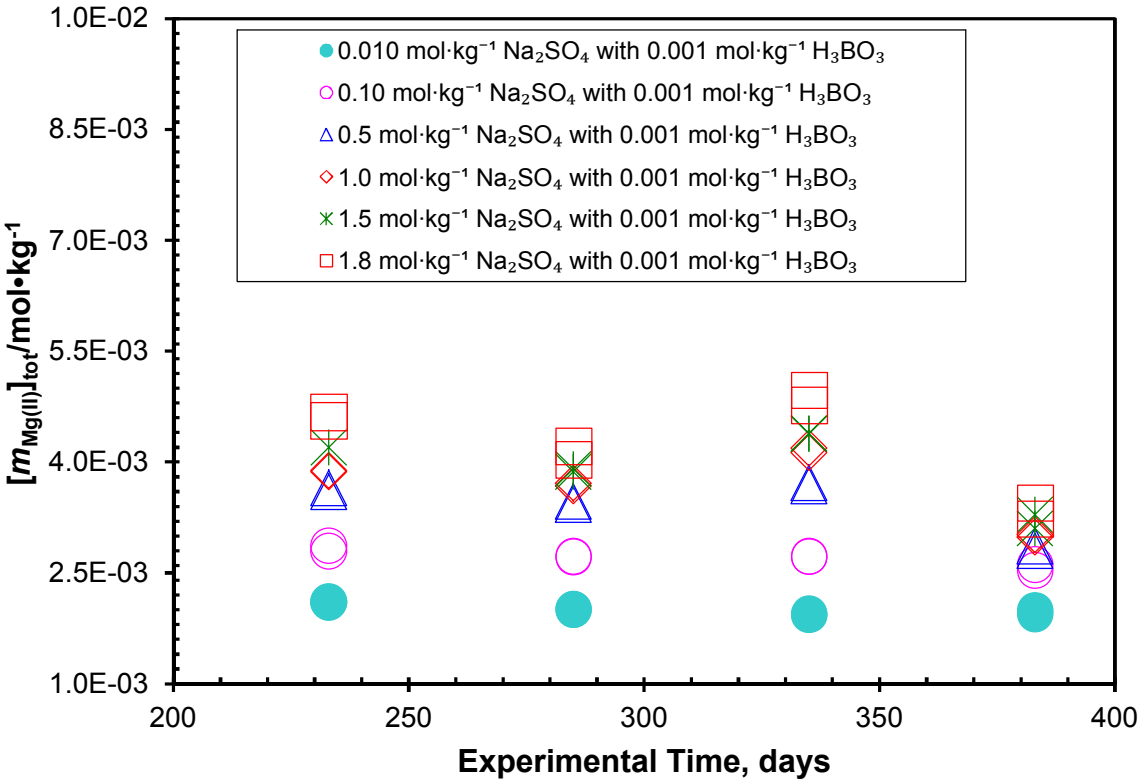

512

513 Figure 2.

514

515

516

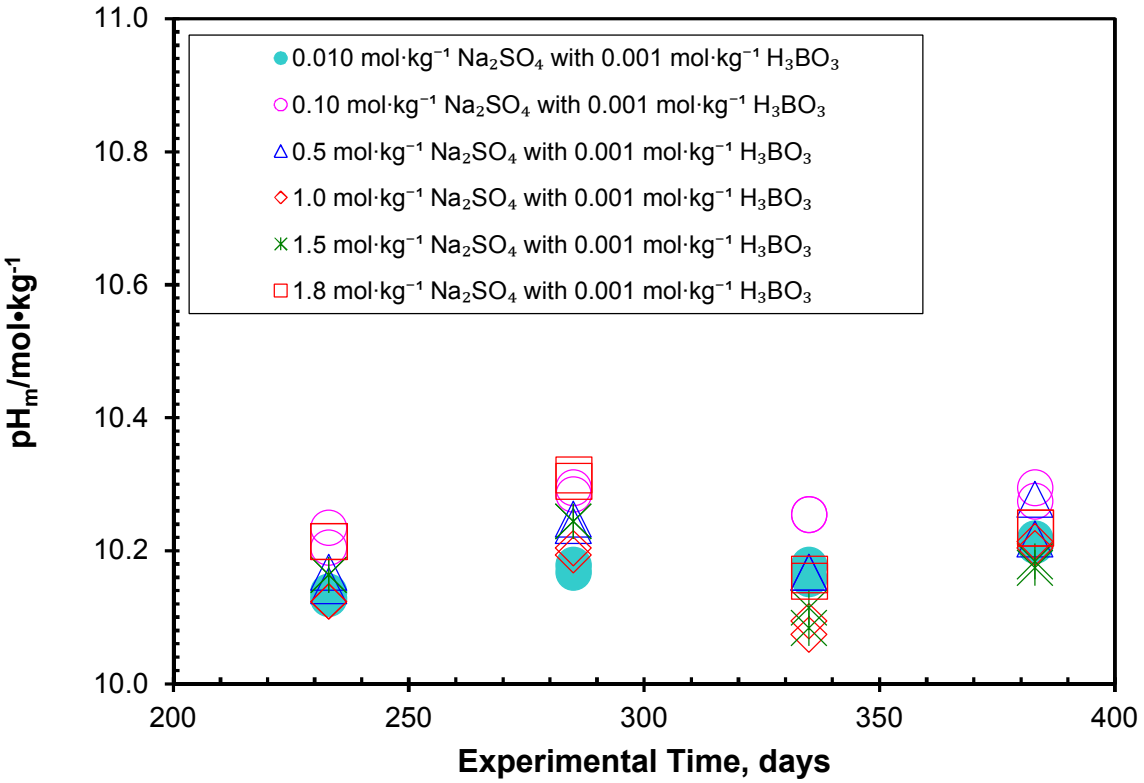

517

518 Figure 3

519

520

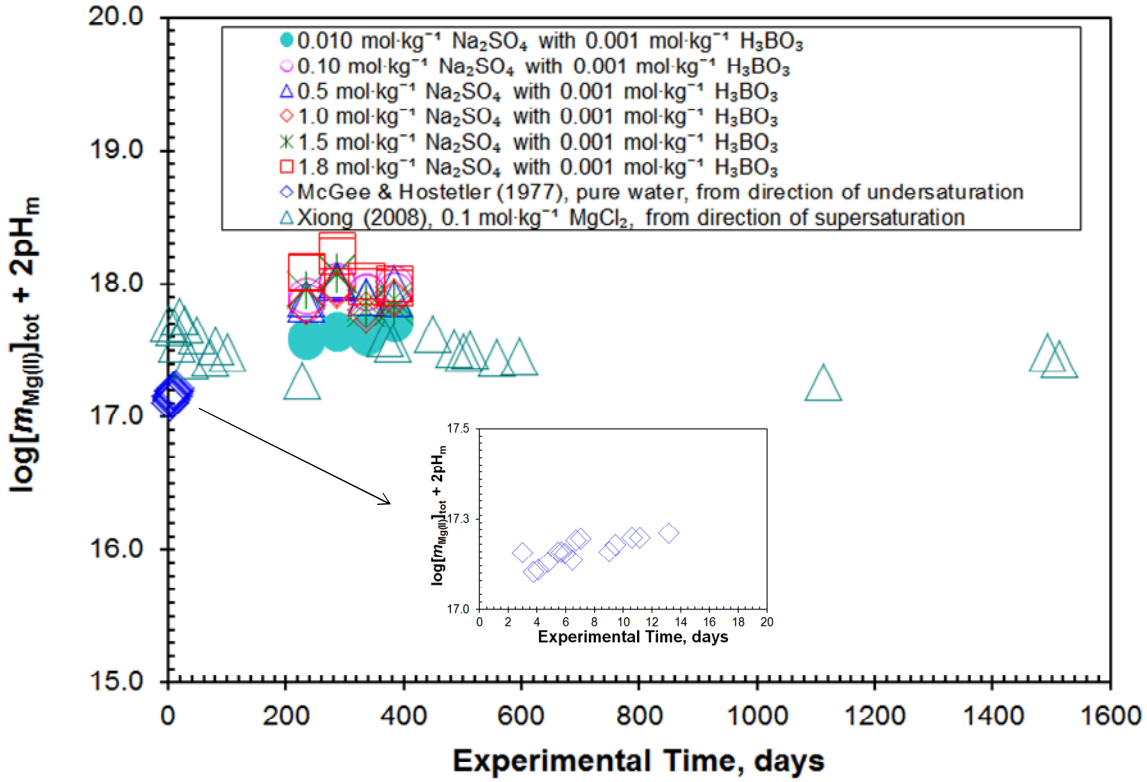

521
522

523 Figure 4.

524
525

526

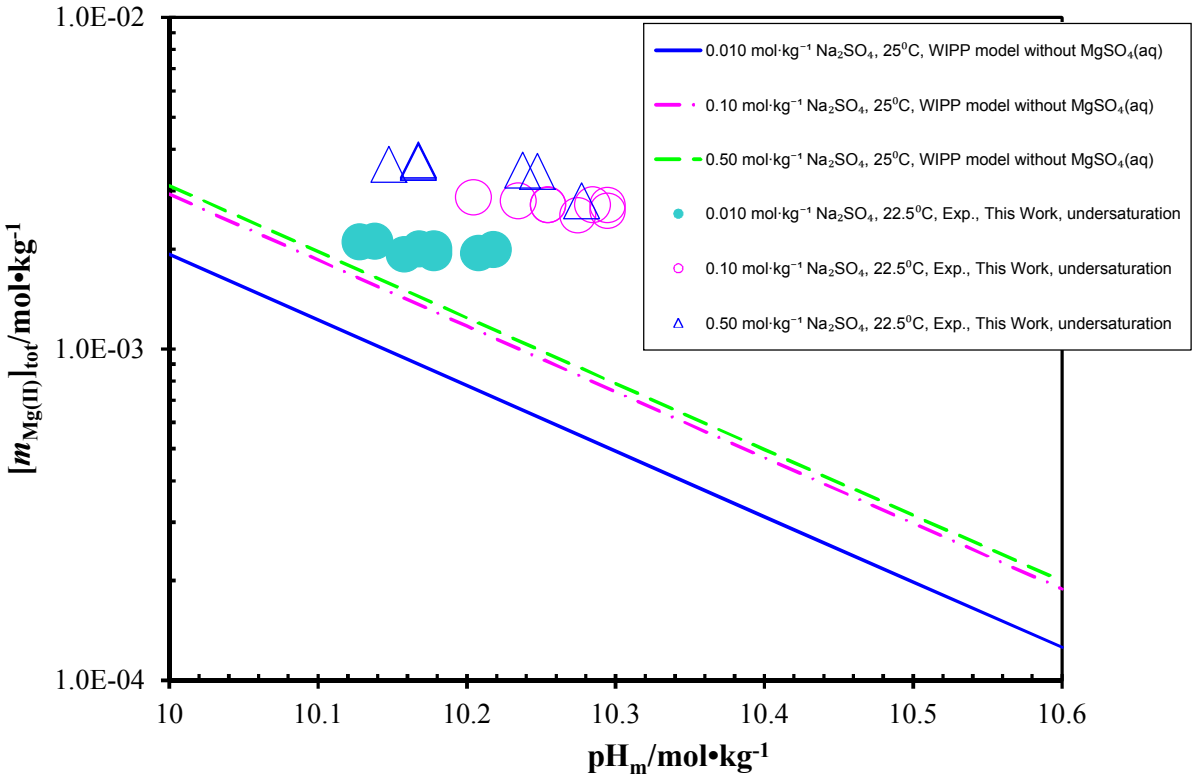

527
528

529 Figure 5.

530

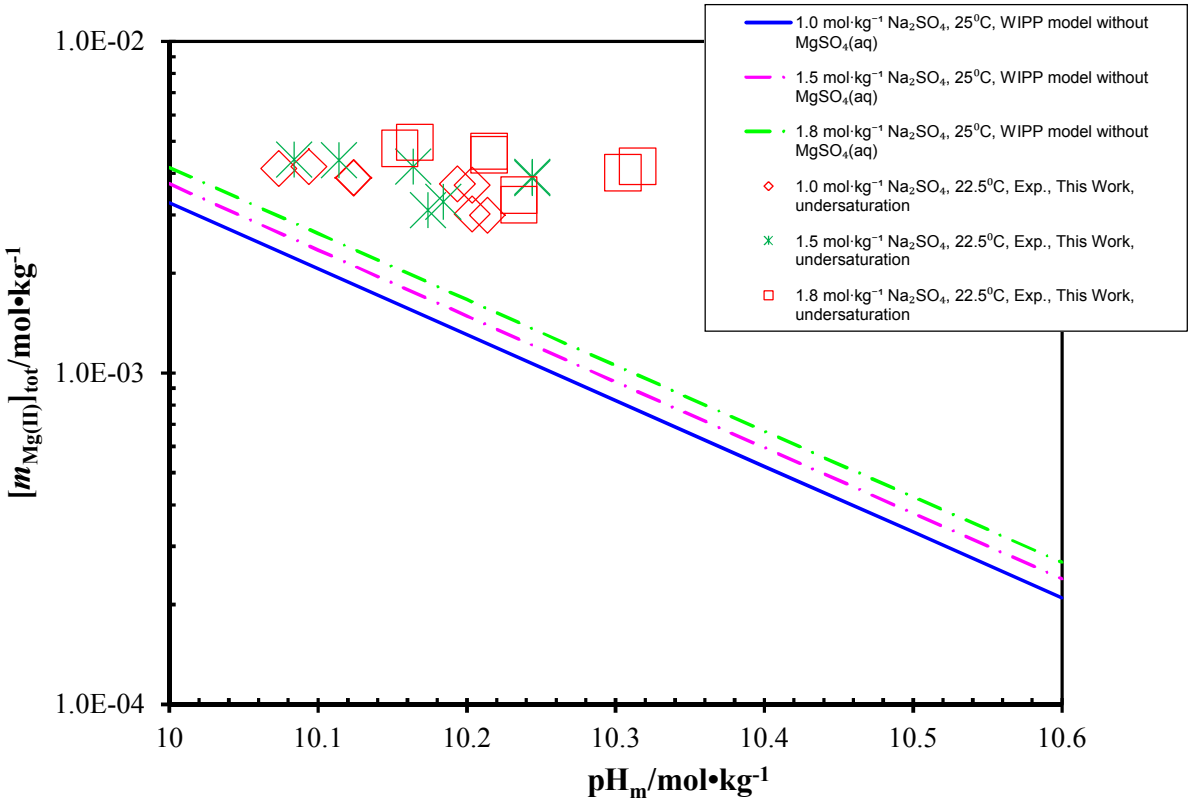
1.0E-02
1.0E-03
1.0E-04
10
10.1
10.2
10.3
10.4
10.5
10.6
$[m_{Mg(II)}]_{tot}$/mol•kg^{-1}
pH$_m$/mol•kg^{-1}
1.0 mol·kg^{-1} Na$_2$SO$_4$, 25^{0}C, WIPP model without MgSO$_4$(aq)
1.5 mol·kg^{-1} Na$_2$SO$_4$, 25^{0}C, WIPP model without MgSO$_4$(aq)
1.8 mol·kg^{-1} Na$_2$SO$_4$, 25^{0}C, WIPP model without MgSO$_4$(aq)
1.0 mol·kg^{-1} Na$_2$SO$_4$, 22.5^{0}C, Exp., This Work, undersaturation
1.5 mol·kg^{-1} Na$_2$SO$_4$, 22.5^{0}C, Exp., This Work, undersaturation
1.8 mol·kg^{-1} Na$_2$SO$_4$, 22.5^{0}C, Exp., This Work, undersaturation

Figure 6.

537
538
539

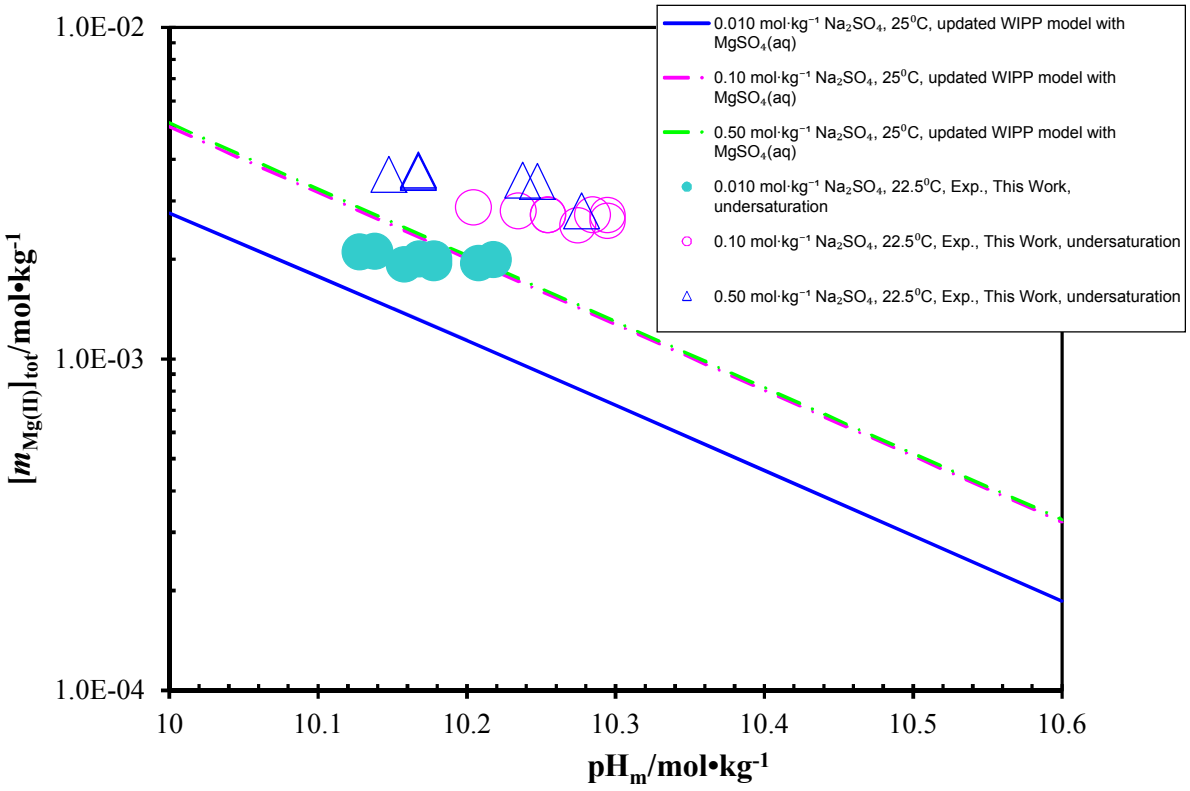

540
541 Figure 7.
542

543

544

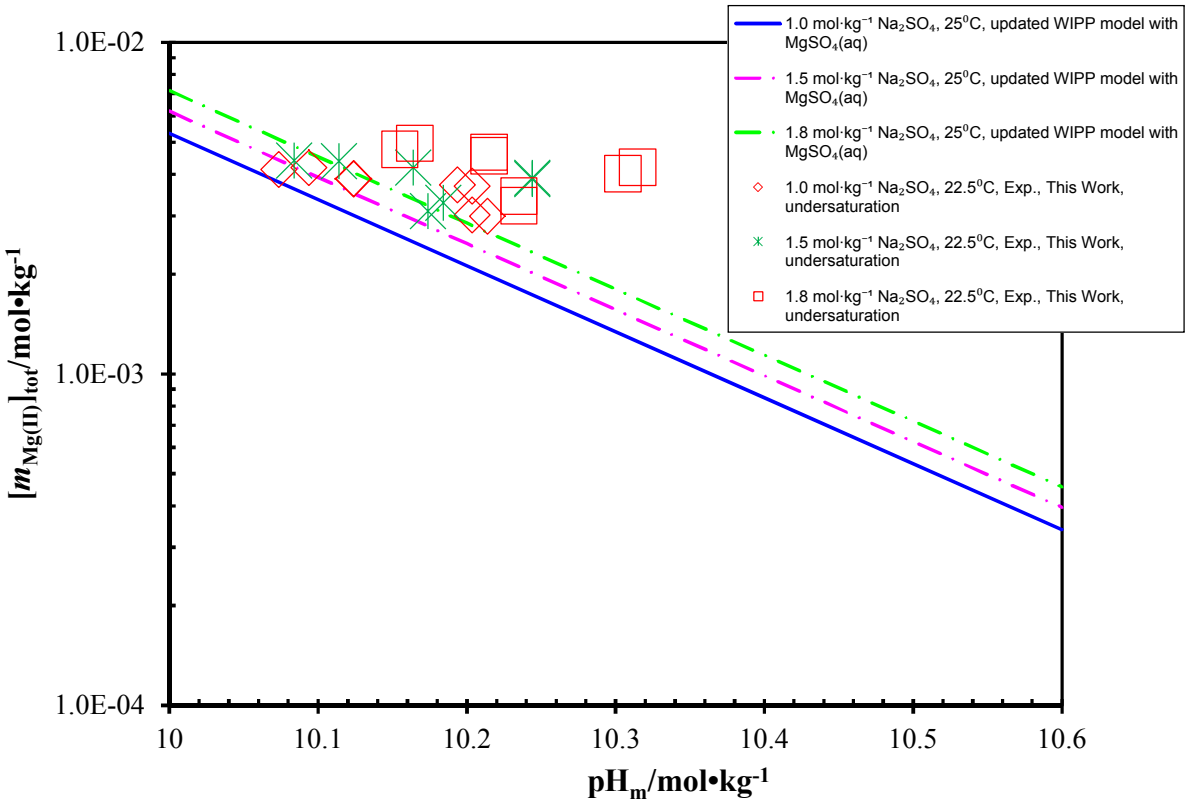

545

546 Figure 8.

547

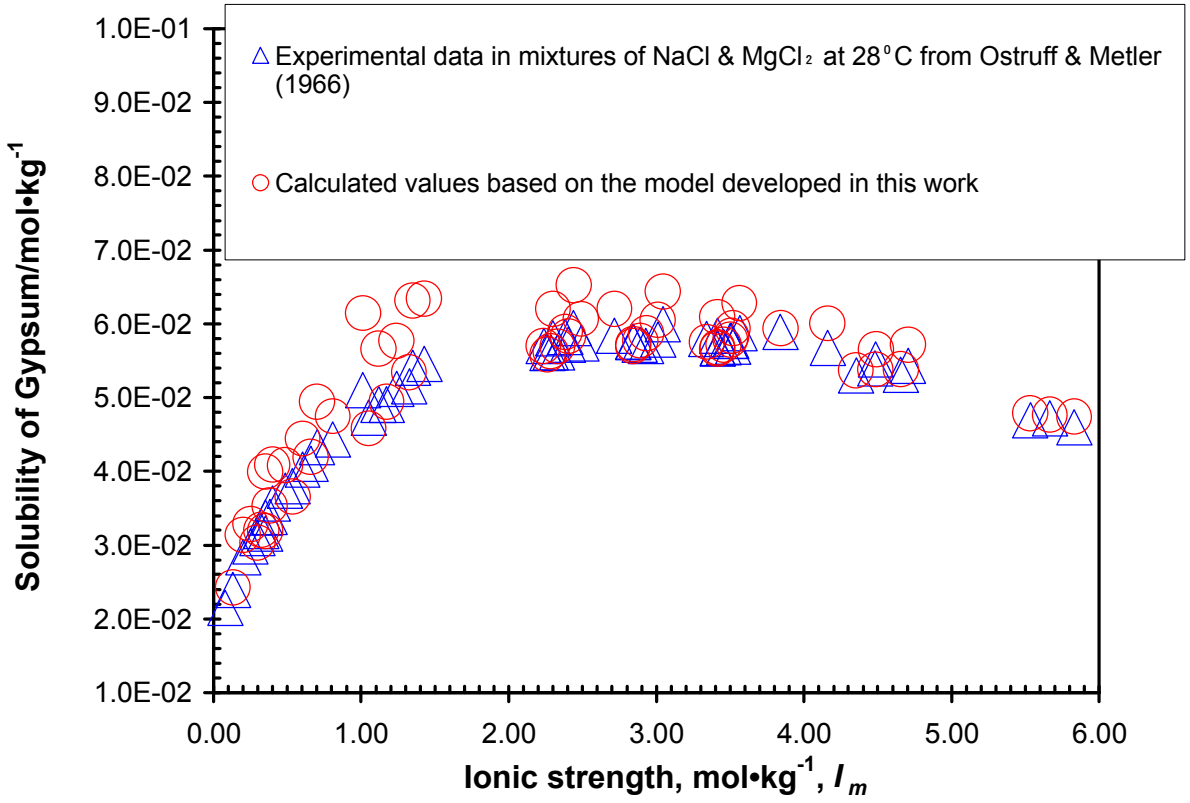

548

549 Figure 9.

550

551

552

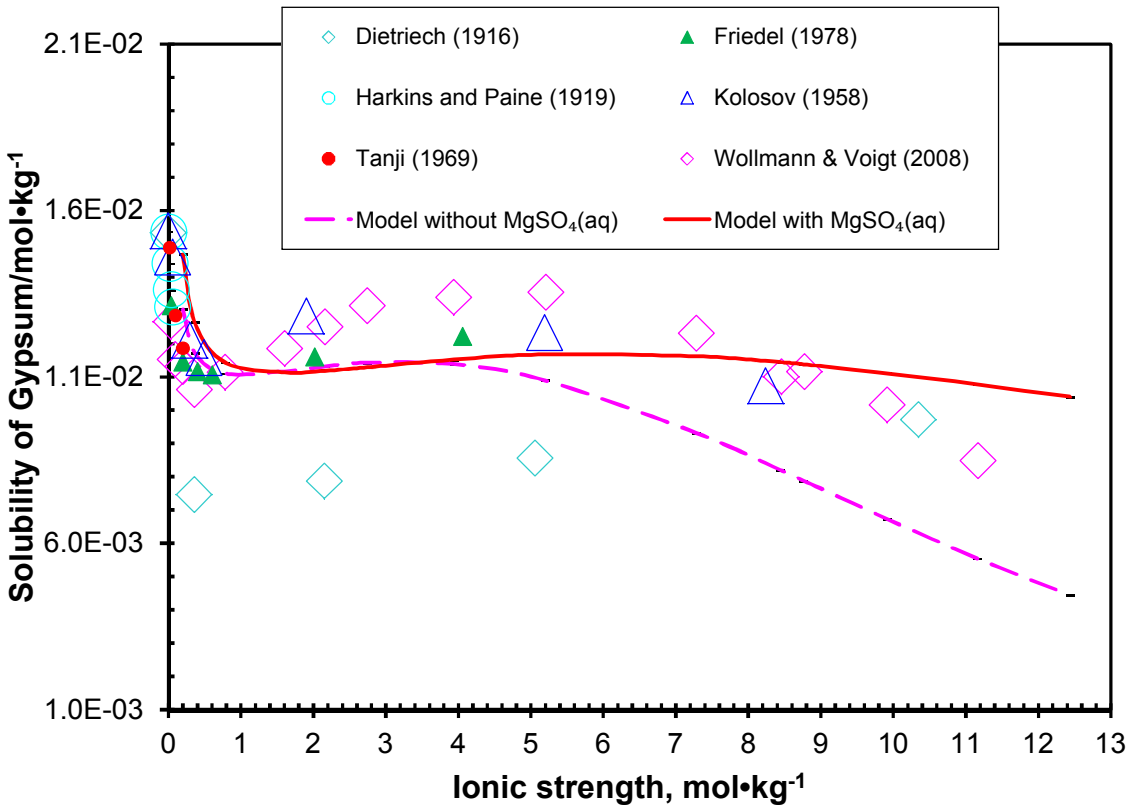

553

554

555 Figure 10.